Unidirectional Allostery in the Regulatory Subunit RIα Facilitates Efficient Deactivation of Protein Kinase A

Cong Guo and Huan-Xiang Zhou*

Department of Physics and Institute of Molecular Biophysics, Florida State University, Tallahassee, FL 32306, USA

*Correspondence e-mail: hzhou4@fsu.edu

Supporting Information

Additional Results

Positional covariance matrices. These matrices were used as input for community analysis. To examine the convergence of conformational sampling for each system and the significance of differences between different systems, following Rivalta *et al*. (1), we carried out statistical analysis on the positional covariance matrices using data from three replicate cMD runs. For each system, the covariance matrices are similar among the three replicate runs, with the SDs (among the replicate runs) of the matrix elements averaging (over all residue-residue pairs) 0.09 for ABbound, 0.13 for Abound, 0.10 for Bbound, and 0.14 for apo (Fig. S2).

We also calculated the average difference matrices between ABbound and the other three systems. A corresponding SD matrix was calculated using all the 9 possible differences crossing the three replicate runs for ABbound and the three replicate runs for each of the other three systems. Inter-domain correlations are of the most interest in the present study. Elements of the average difference matrices for inter-domain residue-residue pairs are shown in Fig. S3, with the pairs of N3A:B with N3A:A and with β-barrel:A, respectively, highlighted by boxes in red and blue dash. Between ABbound and Abound, the differences for these inter-domain pairs are insignificant as their magnitudes are comparable to the average SD of the differences

over all residue-residue pairs (<SD> = 0.16). Relative to ABbound, correlations between N3A:B and β-barrel:A (blue box) decrease by approximately 0.4 while correlations between N3A:B and N3A:A (red box) increase by approximately 0.4. These differences are three times the average SD of the differences (<SD> = 0.14). The decreases and increases of apo in these correlations are approximately 0.5, also three times the average SD of the differences (<SD> = 0.17).

Community structures. The community structure, i.e., the partitioning of communities and inter-community couplings, for replicate Run1 of each system is described in the main text. Here we present the results for Run2 and Run3 (Fig. S4), and highlight the reproducible features among the replicate runs.

For ABbound, Run2 and Run3 are similar to each other in community partitioning and in pattern and strengths of inter-community couplings. Communities 2 and 3 are as strongly coupled as in Run1 (Fig. 3). In Run2, a coupling between communities 1′ and 4 emerges, mediated by 3_{10} loop:A and β1:B. In Run1, 3_{10} loop:A is partitioned to community 1 whereas β1:B is partitioned to community 3. Hence the 1′-4 coupling in Run2 corresponds to a portion of the 1-3 coupling in Run1. Similarly, the 1-4 coupling (mediated by αC/αC′:A and β1/β3/β6/β8:B) in Run3 corresponds to a portion of the 3-4 coupling in Run1.

For Abound, Run2 reproduces well what is shown in Fig. 3 for Run1. In particular, the coupling between communities 2 and 3 dominates in inter-domain communication. In Run3, αB-αC:A and PBC:A merge into a single community, which we now label as 1+2'. The coupling between αA:B and this hybrid community is mostly with PBC:A. In addition, there is significant coupling between community 3' and 2.

For Bbound, Run2 gives the same results as Run1 (Fig. 3). In particular, community 3 couples more strongly to 1 than to 2. In Run3, αA:B is split between communities 3 and 3'. Community 3 is coupled to 1 and 2, while community 3' is coupled to 1 and 1'. The aggregated coupling strength between 3/3' and 1/1' is higher than that between 3 and 2. So qualitatively, Run3 is similar to the other two runs.

For apo, the coupling between communities 2 and 3 is very weak in Run2 and absent in Run3, similar to the counterpart in Run1. In Run2, community 1 is strongly coupled to community 4, mainly due to the presence of αC/αC′:A and parts of αA+β1:B in the former community. In Run3, a coupling between communities 2 and 3′ emerges, but is much weaker than the combined coupling between communities 1/1′ and 3.

Note that community structures are defined not only by which communities are coupled to which other communities, but more importantly defined by how strong the couplings are. Comparing all the replicate runs for all the four systems, the most important reproducible observation is that, in ABbound and Abound, couplings between communities 2/2′ (containing β-barrel:A) and 3/3′ (containing αA/αB:B), highlighted by ovals in red dash in Fig. 3, are stronger than or as strong as those between 1/1′ (containing the helical subdomain of CBD-A) and 3/3′, highlighted by ovals in red dash in Fig. 3, but, in Bbound and apo, the former couplings are either absent or much weaker than the latter coupling.

Comparison between calculated and experimental chemical shift perturbations. Melacini and co-workers (2) used the R209K and R333K mutations to engineer domain-selective perturbations to the doubly bound form. Their backbone amide chemical shift perturbation (CSP) data of the mutants (relative to the wild type) in excess cAMP showed that the mutations affected the chemical shifts of corresponding residues in the two tandem domains to different extents. This observation is corroborated by their H/D exchange data. The latter data were acquired both in excess cAMP and at a cAMP concentration sufficient for binding to the un-mutated CBD but insufficient for binding to the mutated CBD. The differential effects of the two mutations were qualitatively similar at the two cAMP concentrations, but with greater magnitudes at the lower cAMP concentrations. These data suggest that, even with cAMP bound, the mutations significantly disrupt the interactions of the ligand with the binding sites, and therefore the effectiveness of the ligand is compromised and the mutations partially mimic cAMP removal. Because experimental CSP data for singly

bound forms are not available, here we compare our calculated CSPs for Abound and Bbound with the experimental data for the R333K and R209K mutants, respectively.

For Abound, the calculated CSPs are overall small; the values never reach 0.6 ppm (Fig. S5, top panel). This is an indication of the conclusion Abound largely maintains the conformations and dynamics of ABbound. The calculated CSPs are relatively larger in CBD-B an in CBD-A. Larger CSPs occur in the β2-β3 loop, β6, PBC, β8-αB, and αC of CBD-B, which are the same regions where the experimental CSPs of the R333K mutant are the most pronounced (Fig. S5, bottom panel). The calculated CSPs are also relatively large in one CBD-A region, i.e., the β4-β5 loop, although the experimental CSPs are negligibly for CBD-A. The experimental CSPs for several residues (E289, G323, A326, and R333K) exceed 0.6 ppm, perhaps partly reflecting changed close-range interactions of the mutated residue.

The calculated CSPs are overall much larger for Bbound than for Abound, with values for numerous residues exceeding 0.6 ppm, mostly in the β2-β3 loop and PBC of CBD-A (Fig. S6, top panel). These are also the regions where the experimental CSPs of the R209K mutant are the most pronounced (Fig. S6, bottom panel). The calculated CSPs are large in the β4-β5 loop of CBD-B, but the corresponding experimental values for the R209K mutant are negligible.

Recently Melacini and co-workers (3) have also reported chemical shift data for the doubly bound W260A mutant. We calculated the CSPs of the W260A mutant relative to ABbound. Relatively large values are found for residues in N3A, β6, PBC, and the B-C helix of CBD-A, which are the same regions where the experimental CSPs are most pronounced (Fig. S8). In summary, the calculated and experimental CSPs show similar patterns but lack quantitative agreement.

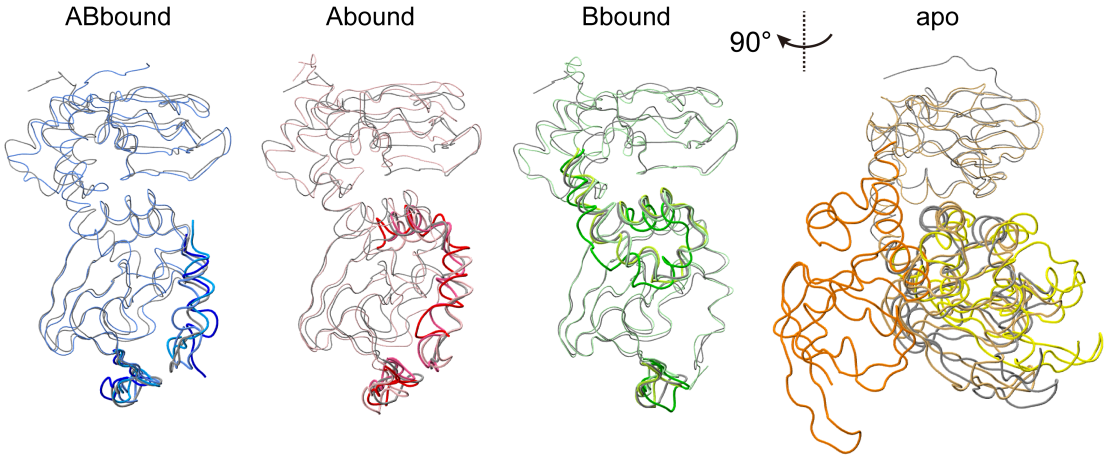

Figure S1. Comparison of the cMD average structures to the crystal structure 1RGS. Cα superposition is over the entire protein for the doubly and singly bound forms and over the β-barrel of CBD-A for the apo form. 1RGS is shown in gray, cMD structures are shown in color. The view for the apo form is rotated 90° from that for the other three systems. For ABbound, Abound, and Bbound, the average structures from three replicate cMD runs are displayed in different shades of blue, red, and green, respectively, for regions showing above-average deviations. These include the β4-β5 loop in CBD-B for all the three bound forms; αB-αC:B for ABbound and Abound; and N3A:B for Bbound. For the apo form, the average structure from one cMD run is shown in light orange, and the B/C helix and CBD-B from the other two cMD runs are shown in orange and yellow.

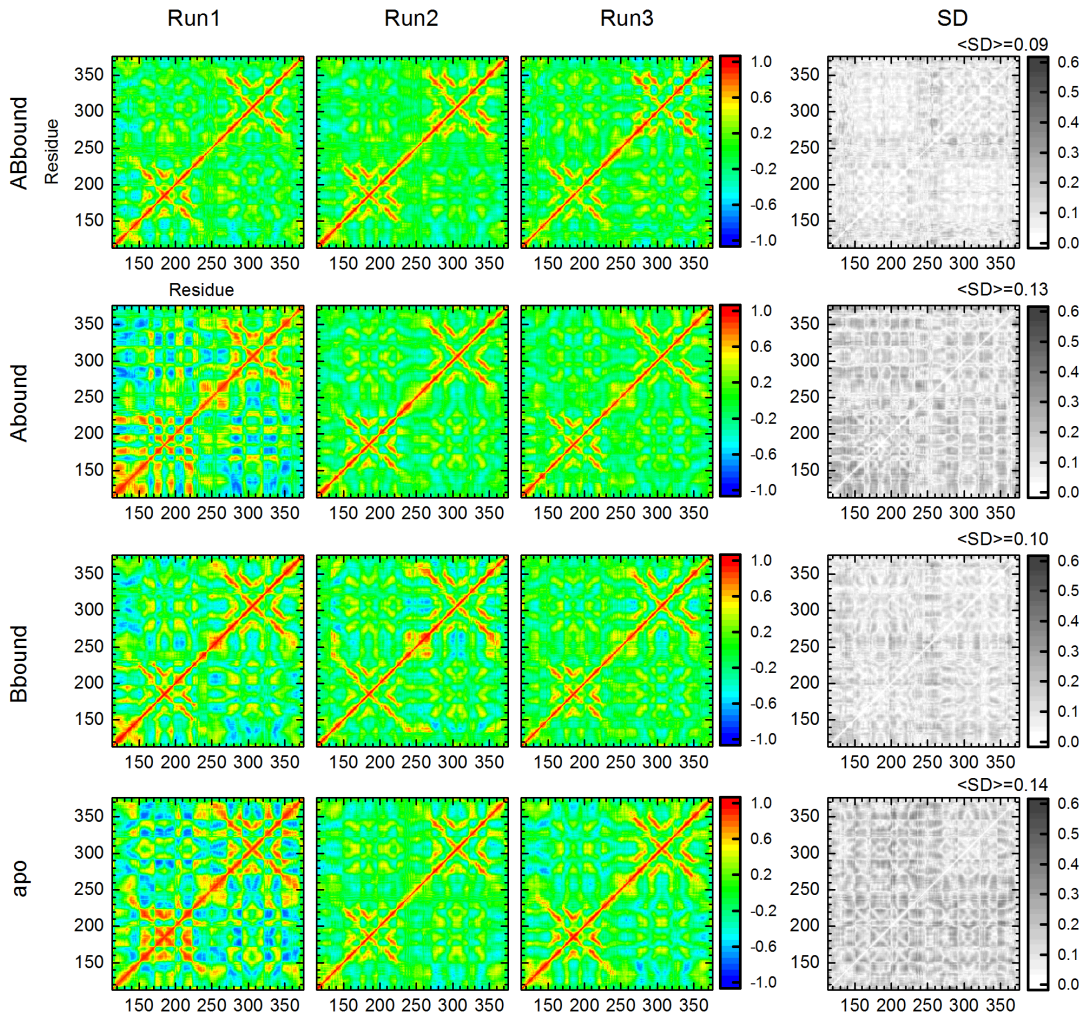

Figure S2. Positional covariance matrices from three replicate runs for ABbound, Abound, Bbound, and apo (from top to bottom). The standard deviations (SDs) of the covariance matrix elements calculated over the three replicate runs are shown on the right. For each system, the average of the SD matrix elements (i.e., <SD>) is listed.

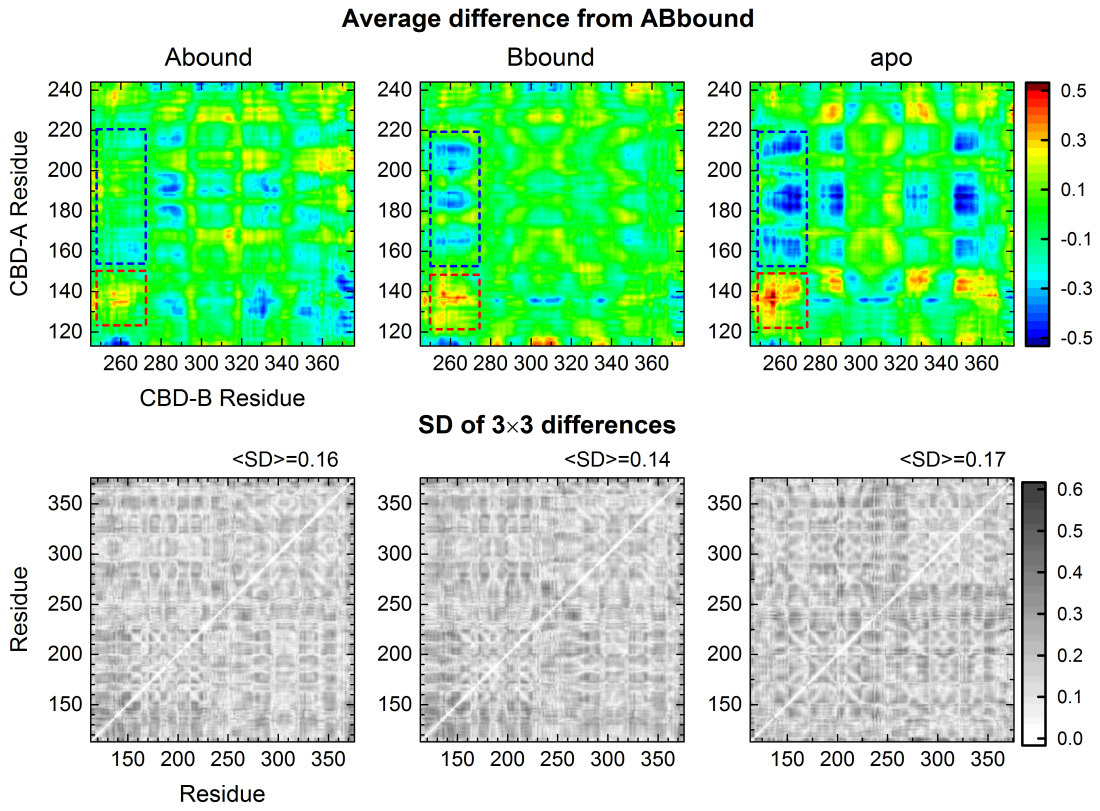

Figure S3. (Top) Difference between the average positional covariance matrix of Abound, Bbound, or apo and the average positional covariance matrix of ABbound. Only the elements of the average difference matrices for inter-domain residue-residue pairs are shown; the pairs of N3A:B with N3A:A and with β-barrel:A, respectively, are highlighted by boxes in red and blue dash. (Bottom) Standard deviations (SDs) of the difference matrix elements, calculated using all the 9 possible differences crossing the three replicate runs for ABbound and the three replicate runs for each of the other three systems. For each system, the average of the SD matrix elements (i.e., <SD>) is listed.

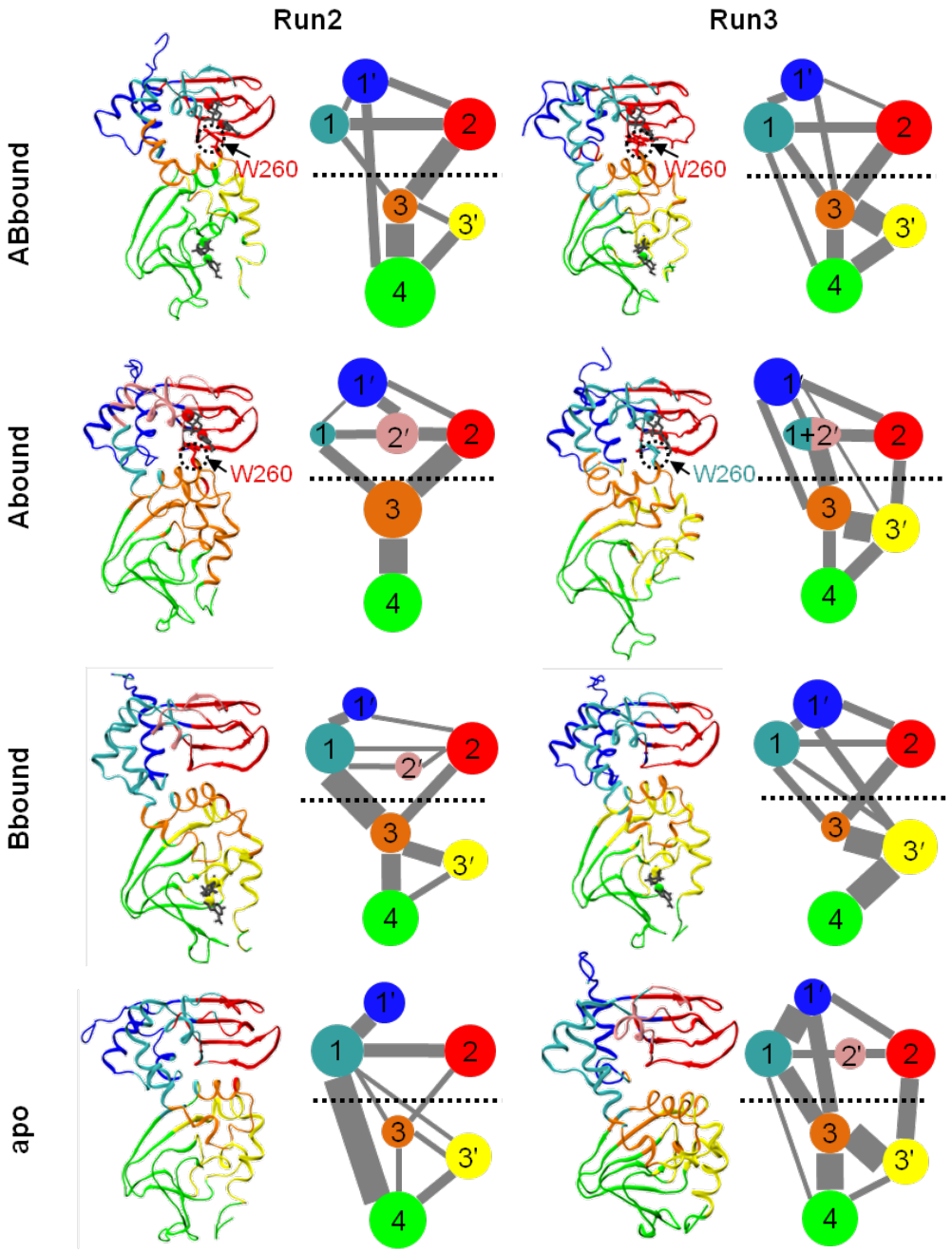

Figure S4. Community analysis for the four systems in two additional cMD runs. For Run3 of Abound, αB-αC:A and PBC:A are in the same community. This community is colored cyan in the left panel, but labeled as 1+2' in the right panel, to highlight the identities of the two regions. The figure legend is otherwise the same as for Fig. 4.

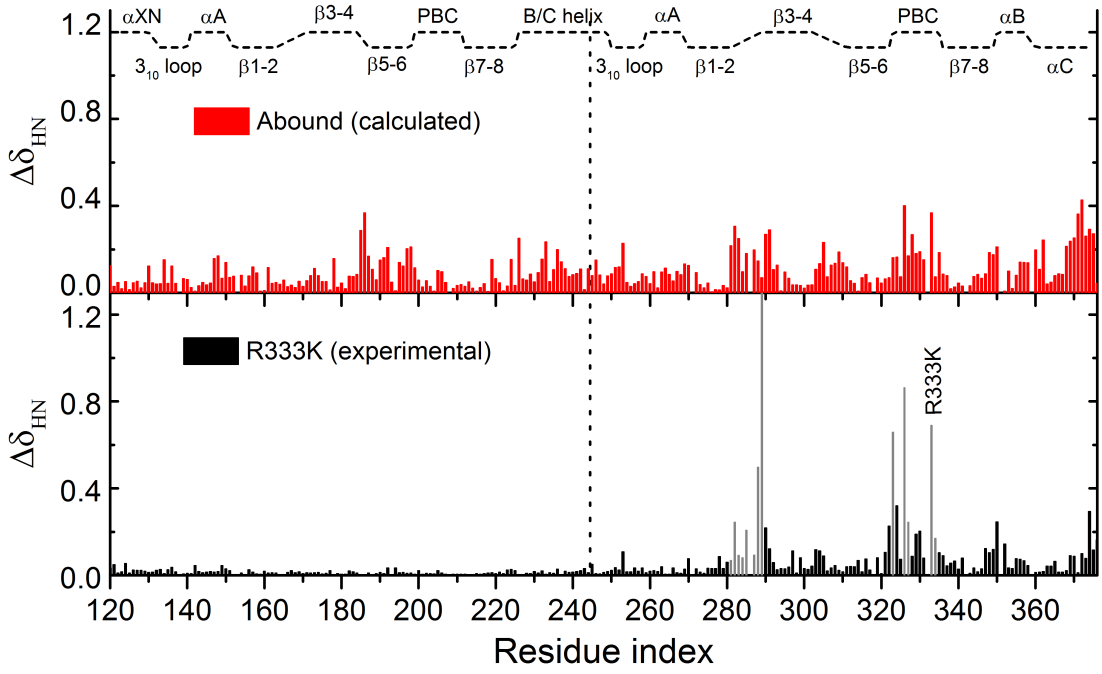

Figure S5. (Top) Backbone amide chemical shift perturbations (CSPs) calculated for Abound (referenced to ABbound). (Bottom) Experimental CSPs for the R333K mutant (2). Gray bars are for residues within 4.5 Å of the mutated residue. Calculated results for residues with missing experimental data are undisplayed in the top panel.

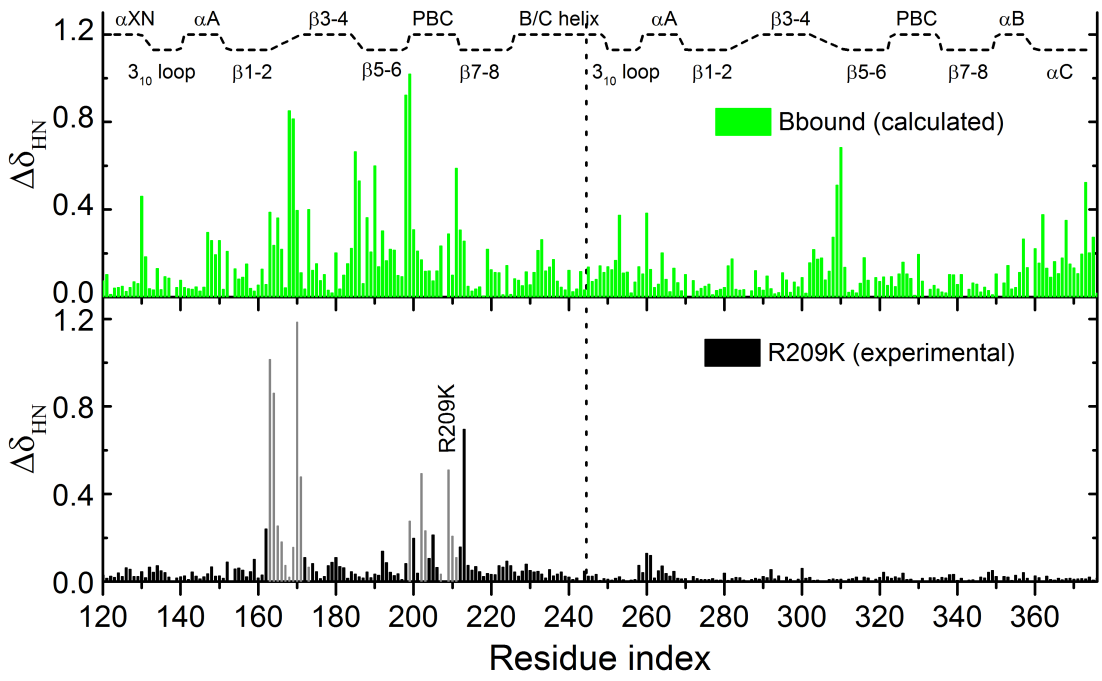

Figure S6. (Top) Backbone amide chemical shift perturbations (CSPs) calculated for Bbound (referenced to ABbound). (Bottom) Experimental CSPs for the R209K mutant (2). Gray bars are for residues within 4.5 Å of the mutated residue. Calculated results for residues with missing experimental data are undisplayed in the top panel.

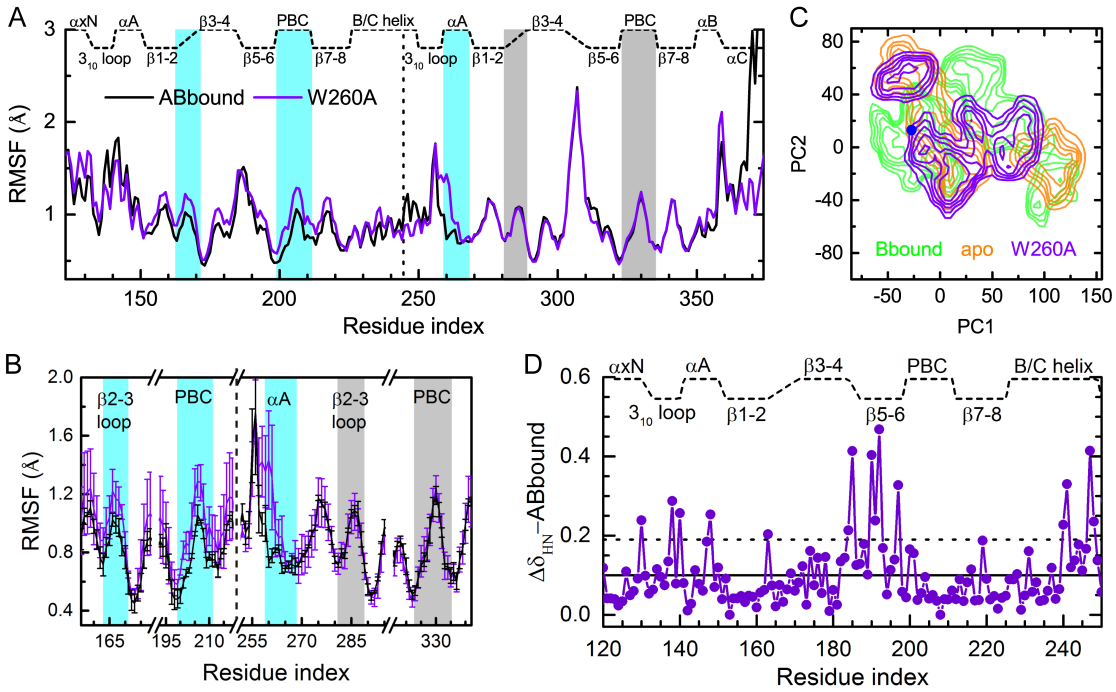

Figure S7. cMD and aMD results for the W260A mutant of ABbound. (*A*) Changes in cMD root-mean-square fluctuation (RMSF) by the mutation. (*B*) RMSF SDs, shown as error bars, for five selected regions. (*C*) Conformational ensemble. aMD snapshots are projected onto the first two principal components of the four wild-type systems, and the resulting probability density in the PC1-PC2 plane is represented as a free energy surface, contoured at 1.5 kcal/mol intervals. Results for Bbound and the apo form are also displayed to serve as reference. (*D*) Backbone amide chemical shift perturbations (CSPs) for CBD-A of the W260A mutant relative to ABbound. The HN CSP of each residue was calculated using the combination formula $\Delta\delta_{HN} = \sqrt{\left(\Delta\delta_H\right)^2 + \left(\Delta\delta_N / 5\right)^2}$ (3). The mean CSP and the value at one standard deviation above the mean are indicated by the horizontal solid and dash lines, respectively.

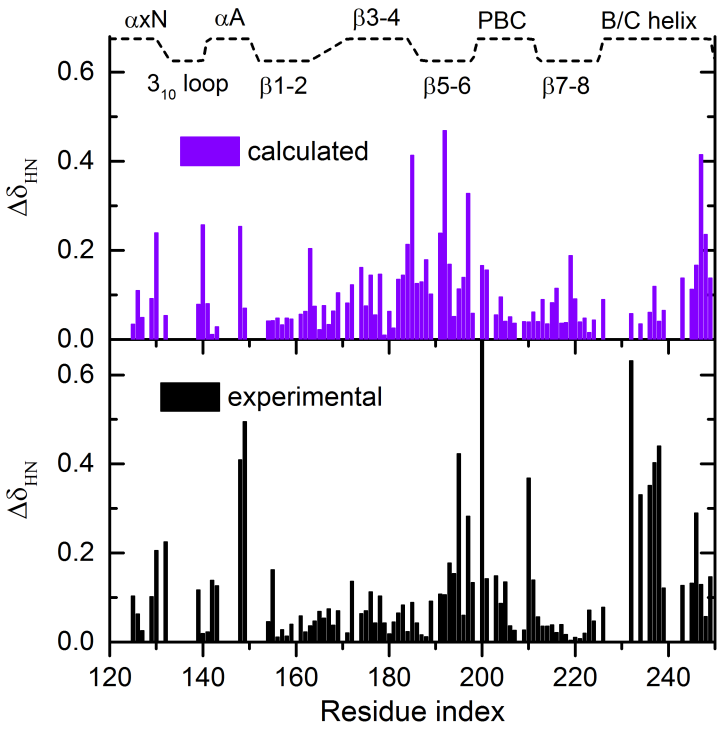

Figure S8. (Top) Backbone amide chemical shift perturbations (CSPs) calculated for CBD-A of the W260A mutant (referenced to ABbound). (Bottom) Experimental CSPs for the W260 mutant (3). Calculated results for residues with missing experimental data are undisplayed in the top panel.

References

1. Rivalta I, *et al.* (2012) Allosteric pathways in imidazole glycerol phosphate synthase. *Proc. Natl. Acad. Sci. U. S. A.* 109(22):E1428-E1436.
2. McNicholl ET, Das R, SilDas S, Taylor SS, Melacini G (2010) Communication between tandem cAMP binding domains in the regulatory subunit of protein kinase A-Iα as revealed by domain-silencing mutations. *J. Biol. Chem.* 285(20):15523-15537.
3. Akimoto M, *et al.* (2015) Mapping the free energy landscape of PKA inhibition and activation: A double-conformational selection model for the tandem cAMP-binding domains of PKA RIα. *PLoS Biol.* 13(11):e1002305.